BULLETIN OF THE POLISH ACADEMY OF SCIENCES
TECHNICAL SCIENCES, Vol. 73(4), 2025, Article number: e154273
DOI: 10.24425/bpasts.2025.154273

Numerical simulation method of fork-flow condenser and the influence of fin structure characteristics

Kaiming LIU[1], Nianyong ZHOU[1]*, Lianghui LIU[1], Benshi HAN[2], Jing LI[1], Guanghua TANG[2], Jixiang LIU[1], and Feifei WANG[1]

[1] School of Urban Construction, Changzhou University, Changzhou, China
[2] Xinxiang Aviation Industry Group Co. LTD, Xinxiang, 453049, China

Abstract. Many researchers have investigated numerical simulation methods for two-phase flow in condensers. Still, challenges persist due to these models' large size, complex structure, and multiphase flow fields. To address these issues, this paper employs a periodic iterative numerical simulation approach for ultra-long condensers, validating the method through experiments and advancing the numerical simulation technology for such models. The study emphasizes the impact of structural changes on the refrigerant and air sides. Results indicate that the most minor error occurs when the number of iterations in the two-phase zone does not exceed three. Increasing the total number of refrigerant channels from 10 to 18 enhances heat transfer by 17.7% and condensation capacity by 10.6%. However, further increases in channel numbers lead to a significant rise in pressure drop, deteriorating heat transfer performance. Heat transfer and condensation capacity improve with the height-to-width ratio of the refrigerant channel, reaching optimal performance when the ratio is close to 1. Additionally, increasing the aspect ratio on the air side will improve the heat transfer and condensation rate of the condenser. However, when the aspect ratio reaches 4.53, further increases will lead to a decrease in the heat transfer coefficient and an increase in pressure drop.

Keywords: condenser; multiphase flow; periodic iteration; numerical simulation; heat transfer characteristics.

NOMENCLATURE

Symbols

u	Velocity, $m \cdot s^{-1}$
S	Source term
K	Heat transfer coefficient, $W \cdot cm^{-2} \cdot {}^{\circ}C^{-1}$
g	Gravitational acceleration, $m \cdot s^{-2}$
F	Force, N
C_v	Gas-phase curvature
C_l	Liquid-phase curvature
E	Energy, $W \cdot m^{-3}$
P	Pressure, Pa
k	Thermal conductivity, $W \cdot m^{-1} {}^{\circ}C^{-1}$
T	Temperature, K
LH	Latent heat, $kj \cdot kg^{-1}$
Fa	Effective heat transfer area on the air side, m^2
t	Time, s

Greek symbols

σ_{lv}	Surface tension, $N \cdot m^{-1}$
α	Volume fraction
μ	Dynamic viscosity, $N \cdot s \cdot m^{-2}$
β	Empirical frequency constant, s^{-1}
ρ	Density, $kg \cdot m^{-3}$
ε	Aspect ratio

Subscripts

n	Number
v	Vapor phase
l	Liquid phase
mix	Two-phase mixing
sat	Saturation
in	Inlet
out	Outlet
M	Mass
co	Condensation

Abbreviations

CPE	Comprehensive performance evaluation factor

1. INTRODUCTION

With the improvement in socioeconomic conditions, there has been a significant advancement in the development of automobiles, airplanes, and other modes of transportation. This progress has, in turn, increased the demand for high-quality research and development of related components, such as condensers and heat exchangers. The condenser is a crucial heat exchange component in thermal management systems used in aviation, vehicles, and various other applications. Enhancing the heat exchange efficiency of the condenser can markedly improve the refrigeration effect and overall energy efficiency of the system [1]. Current development trends for onboard thermal management systems in machinery, including vehicles, emphasize miniaturization, lightweight design and high efficiency [2].

*e-mail: zhounianyong@cczu.edu.cn

Manuscript submitted 2024-09-05, revised 2025-03-15, initially accepted for publication 2025-03-20, published in July 2025.

During the second stage of heat transfer, specifically in the gas-liquid two-phase region, Peker *et al*. [3] conducted experimental studies on how variations in tube shape affect heat transfer in a thermal wall condenser. Their findings revealed that changes in tube cross-sectional shape (O/D) enhanced the heat transfer rate, with improvements ranging from O to D. Specifically, doubling the flow velocity and increasing the condenser tube diameter resulted in an average heat transfer rate increase of 8.9% and 5.2%, respectively. Şahnali *et al*. [4] pioneered the use of the Kammtail shape instead of circular or elliptical geometries in finned tube heat exchangers. Through experiments and numerical analysis, they demonstrated the advantages of this shape, with the 3×6 mm Kammtail shape showing a 19% reduction in pressure drop and over a 9% increase in the heat transfer coefficient as compared to the circular tube profile. Espindola *et al*. [5] explored the correlation between air-side heat transfer coefficients in natural ventilation tubes used in household refrigeration with various geometric designs. They found that combined heat transfer coefficients are highly sensitive to wire spacing; shorter wire spacing leads to constraint effects, reducing shape factors and buoyancy, which in turn decreases radiation and convective heat transfer efficiency. Ammar *et al*. [6] conducted a detailed experimental study on the condensation heat transfer in human-shaped plate heat exchangers (PHEs) used in absorption refrigeration systems. They highlighted the significant impact of inlet temperature and saturation pressure on the heat transfer coefficient (HTC) and heat flux. An increase in inlet temperature decreased heat flux, although HTC remained relatively unchanged at saturated pressure. Comparing PHEs with shell-and-tube heat exchangers, they found that the human-shaped plate condenser exhibited excellent heat transfer performance but experienced increased pressure drop due to turbulent flow. Yan *et al*. [7] investigated the heat transfer coefficient and pressure drop during condensation in small pipes with a diameter of 2 mm. They observed lower heat transfer coefficients and pressure drops at higher saturation temperatures of refrigerants. Webb *et al*. [8] tested pressure drop and heat transfer in compact tube-in-fin heaters with hydraulic diameters of 1.56 mm and 2.64 mm. Their results showed that pressure drop increased within the finned tubes as the R12 refrigerant condensed, with a continuous rise in pressure drop as the liquid volume fraction decreased. Chung *et al*. [9] analyzed flow and heat exchange in parallel flow heaters using two different-sized models. They concluded that having nine fins per pass resulted in optimal thermal performance among the four configurations tested. Bullard *et al*. [10] designed microchannel plate fin evaporators and condensers using R410A refrigerant with varying numbers of finned tubes (38, 24, 9). They reported a 25% reduction in power consumption as compared to baseline models. Cavallini *et al*. [11] investigated frictional pressure dropped when R134a, R236ea, and R410A refrigerants flowed through microchannel condenser tubes under two-phase flow conditions. Their results showed significantly lower pressures in R410A tubes as compared to R134a or R236ea tubes under similar conditions. Additionally, the R134a results were consistent with those reported by Zhang and Webb [12] and Webb and Ermis [13]. Wang *et al*. [14] tested 12 types of fins with varying specifications to investigate the effects of air-side fin spacing and the number of tube rows on heat exchange performance. They found that reducing fin spacing with a single tube row improves heat transfer performance. However, with more than four tube rows, reducing fin spacing actually decreases performance. Additionally, increasing the number of tubes leads to decreased heat transfer efficiency. Du *et al*. [15] explored the effects of four air volume inlet angles (30°, 45°, 60°, and 90°) on heat transfer and pressure drop, finding that a decrease in inlet air angle reduces heat transfer capacity at a constant mass flow rate. Kim *et al*. [16] tested nine configurations under dry conditions, including herringbone and smooth corrugated fins paired with round and oval tubes. The results showed that smooth corrugated fins with elliptical tubes had superior heat transfer and friction factors as compared to other combinations, attributed to their higher thermal conductivity and increased pressure drop. Jabardo *et al*. [17] studied the impact of air-side louvre fins and wavy fins on heat transfer performance in parallel flow heat exchangers. They found that within Reynolds numbers of 1000 to 6000, the spacing of these fins has minimal impact on heat transfer efficiency. Ryu [18] observed that the correlation between fin spacing (Fp) and louvre spacing (Lp) is not valid for Fp/Lp > 1. His findings suggest that within the Reynolds number range of 100 to 3000, heat transfer factor j and friction factor f exhibit universality only when Fp/Lp > 1.

In summary, past research has predominantly utilized experimental methods to investigate the impact of fin structure, channel quantity, and system parameters on condenser heat transfer. Numerical simulation studies for large condensing channels remain sparse. This study developed a physical model of a fork-flow condenser using two-phase flow theory and explored numerical simulation techniques. It examined how channel aspect ratio and quantity influence heat transfer characteristics, and then assessed the overall performance of the condenser.

2. STUDY ON NUMERICAL SIMULATION METHOD OF CONDENSING HEAT TRANSFER IN FORK-FLOW CONDENSER

2.1. Establishment of a physical model of fork-flow condenser

This paper details a numerical simulation of a fork-flow condenser used in an airborne thermal management system. The condenser is divided into four stages with 22, 16, 7 and 6 refrigerant channels, respectively. It has external dimensions of 500 mm × 360 mm × 18.9 mm (length × width × height). Each single-layer heat exchange channel measures 360 mm × 18.9 mm × 6.5 mm. Specifically, with 22 channels, each refrigerant channel is 360 mm long, with the dimensions of 0.65 mm × 0.9 mm. The fin size is 18.9 mm × 0.07 mm × 2.55 mm, with a spacing of 1.15 mm. To save computational effort during simulation, a half-length of 180 mm was chosen for grid independence verification (Fig. 1).

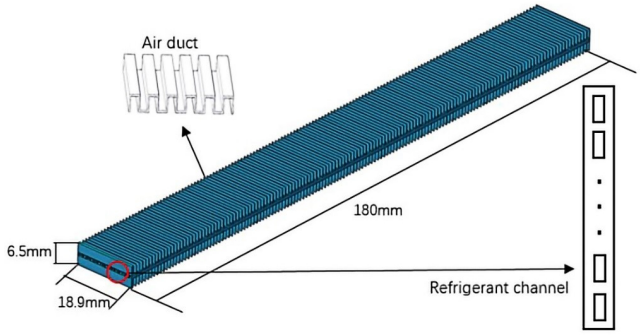

Fig. 1. Simplification of a physical model of the condenser

2.2. Mathematical models and data processing

In the calculation of multiphase flow, the Euler-Euler method is used because it incorporates the concept of phase volume fraction, treating each phase as a continuous medium that interacts with others. This method solves the Navier-Stokes equations to track the flow behavior of each phase. The Navier-Stokes equations describe the interactions between liquid and gas phases and include mathematical formulations for mass continuity, momentum, and energy [19].

Continuity equation:

$$\frac{\partial(\alpha_l \rho_l)}{\alpha_t} + \nabla \cdot (\alpha_l \rho_l \vec{u}) = S_M \,. \tag{1}$$

Momentum equation:

$$\frac{\partial(\rho \vec{u})}{\partial_t} + \nabla \cdot (\rho \vec{u}\,\vec{u}) = -\nabla P + \nabla \cdot \left[\mu\left(\nabla \vec{u} + \nabla \vec{u}^T\right)\right] + \rho \vec{g} + \vec{F}_{CSF} \,. \tag{2}$$

$\vec{F}_{CSF}$ is expressed as the surface force of a continuous medium, while Brackbill *et al.* [20] proposed a continuous medium surface tension model, as shown below:

$$F_{CSF} = 2\sigma_{lv} \frac{\alpha_l \rho_l C_v \nabla \alpha_v + \alpha_v \rho_v C_l \nabla \alpha_l}{\rho_l + \rho_v} \,. \tag{3}$$

Energy equation:

$$\frac{\partial(\rho E)}{\partial_t} + \nabla \cdot \left[\underset{u}{\rightarrow}(\rho E + P)\right] = \nabla \cdot (k \nabla T) + S_E \,. \tag{4}$$

Phase transition equations during the condensation process:

$$S_M = \beta_{co} \alpha_v \rho_v \frac{T_{sat} - T_{mix}}{T_{sat}} \,, \tag{5}$$

$$S'_{Mv} = -S_{Mv} \,, \tag{6}$$

$$S_E = \beta_{co} \alpha_v \rho_v \frac{T_{sat} - T_{mix}}{T_{sat}} \cdot LH. \tag{7}$$

Heat transfer coefficient of the condenser:

$$K = \frac{Q}{F_a \Delta t_m} \,. \tag{8}$$

Condenser heat transfer temperature difference:

$$\Delta t_m = \frac{t_2 - t_1}{\ln \dfrac{\bar{t}_{in} - t_1}{\bar{t}_{in} - t_2}} \,. \tag{9}$$

Considering the overheating and undercooling of the refrigerant at the inlet and outlet of the condenser, the average temperature of the refrigerant inside the condenser can be expressed by the following equation:

$$\bar{t}_{in} = \frac{t_{in} + t_{out}}{6} + \frac{2t}{3} \,. \tag{10}$$

A comprehensive performance evaluation factor, commonly referred to as CPE (comprehensive performance evaluation), is used to assess the performance of a condenser. Generally, a higher CPE value indicates better condenser performance. The CPE is represented as:

$$CPE = \frac{K}{\Delta P^{\frac{1}{3}}} \,. \tag{11}$$

2.3. Grid independence verification

In the example of a 180 mm condenser, six sets of grids are generated with quantities of 2.1 million, 3.5 million, 4.7 million, 5.5 million, 6.5 million, and 7.1 million, respectively. We have fully considered the $y+$ parameter, and for the standard k-Epsilon model, the recommended value of $y+$ is ideally close to 30. According to the $y = (y^+\mu) \times (\rho\mu^*)^{-1}$ formula, the height y of the first layer is approximately 7.8e-5m by calculation. Therefore, in the grid model, the grid height of the first layer is controlled at 7.8e-5m, and the second layer and above will be increased by a factor of 1.2.

Using an inlet temperature of 330K for R134a refrigerant on the wind side and 313 K for the air, the condensation amount and outlet temperature of the R134a refrigerant are evaluated to check grid independence. As shown in Fig. 2, the results for condensation amount and outlet temperature begin to stabilize when the grid number reaches 5.5 million, with further increases having a negligible impact on the simulation results. Consequently, the final number of simulation grids is determined to be 5.5 million.

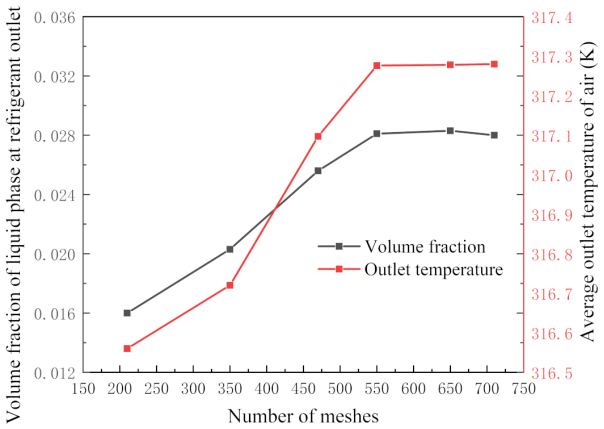

Fig. 2. Verification of refrigerant channel independence in condenser

3. VERIFICATION OF PERIODIC ALTERNATIVE NUMERICAL SIMULATION METHOD

Due to the large overall volume and long refrigerant channels of the condenser, simulating the entire system poses significant challenges. Therefore, a periodic iteration method is employed for the simulation, and in order to save computational resources and quickly verify the pattern, one-third of the length of the condenser flow, namely 120 mm, was chosen as the reference length for the calculation. To validate the accuracy of the two-phase zone periodic iteration simulation method, the condenser is initially simulated as a whole. It is then divided into 2, 3, and 4 sections for iterative calculations, with the outlet parameters of one section serving as the inlet parameters for the subsequent section, as shown in Fig. 3. The simulation parameters are as follows: refrigerant inlet flow rate is 1.43 kg/h, refrigerant inlet temperature is 330 K, air inlet velocity is 5 m/s, and air inlet temperature is 313 K.

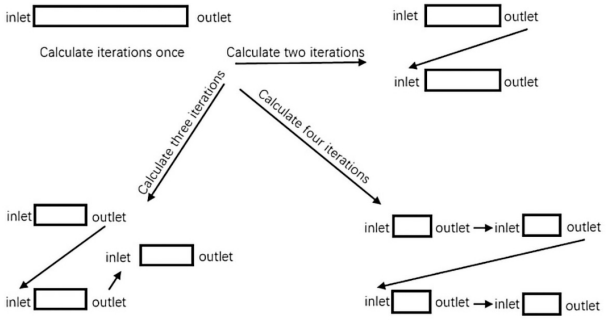

Fig. 3. Schematic diagram of condenser cycle iteration model

As shown in Table 1, after simulating the 12 0mm reference model, the average refrigerant outlet temperature is 323.95 K, the average air outlet temperature is 315.72 K, and the total heat transfer of the condenser is 7.87 W. The relative errors in the refrigerant outlet temperature after 2, 3, and 4 iterations were 0.03%, 0.19%, and 0.31%, respectively, with errors within 0.02 K. The relative errors for refrigerant heat transfer were 0.25%, 0.76%, and 1.27%, with the heat transfer error not exceeding 0.03 W. The relative errors for condensation amounts were 0.43%, 1.02%, and 2.32%, with the error not exceeding 0.016. Table 2 illustrates that the error between the iterative calculations of the condensation amount at each refrigerant outlet and the original simulation model's values is minute.

Table 2
Verification of periodic iteration calculation in two-phase zone

Iteration times	R134a flow length (mm)	Cloud map of liquid phase volume fraction at the refrigerant outlet
1	0–120	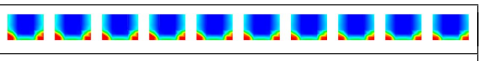
2	0–60	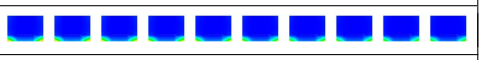
	60–120	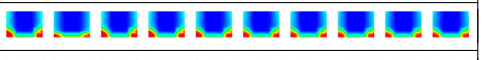
3	0–40	
	40–80	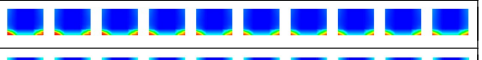
	80–120	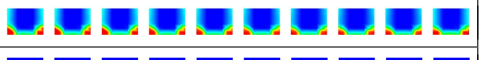
4	0–30	
	30–60	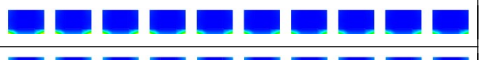
	60–90	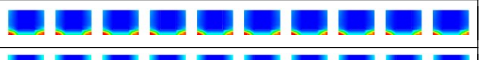
	90–120	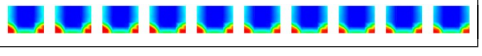

In summary, the use of periodic iteration technology results in minimal error between the simulation results and the overall

Table 1
Analysis of periodic iteration error in two-phase zone

Iteration times	Flow length of R134a (mm)	Inlet temperature of R134a (K)	Average outlet temperature of R134a (K)	Inlet temperature of air (K)	Outlet temperature of air (K)	Volume fraction of liquid phase at the outlet (%)	Total heat exchange (W)
1	0–120	330	323.95	313	315.72	0.69	7.87
2	0–60	330	323.98	313	315.84	0.16	7.85
	60–120	330	323.95	313	315.59	0.68	
3	0–40	330	324.00	313	315.99	0.10	7.81
	40–80	330	323.98	313	315.56	0.53	
	80–120	330	323.96	313	315.60	0.68	
4	0–30	330	324.00	313	316.11	0	7.77
	30–60	330	323.98	313	315.58	0.15	
	60–90	330	323.97	313	315.58	0.41	
	90–120	330	323.97	313	315.60	0.67	

model results. By decomposing a large model into multiple simulations, computing resources are used more efficiently, and simulation calculation times are significantly reduced. However, it was observed that increasing the number of iterations leads to an increase in calculation error. Based on a comprehensive evaluation, it is recommended to perform no more than three iterations. For future simulations, a maximum of two iterations is advised.

4. EXPERIMENTAL VERIFICATION AND INFLUENCE OF CHANNEL STRUCTURE ON HEAT TRANSFER CHARACTERISTICS

4.1. Experimental verification and analysis of numerical simulation of condenser

To ensure the accuracy of simulation calculations, this study integrates experimental testing with simulation methods to validate their effectiveness. This approach involved collecting experimental data to corroborate the accuracy of the condenser simulation method. The schematic diagram of the condenser system is shown in Fig. 4.

To keep the simulation conditions consistent with the experimental conditions, at the start of the experimental test, the refrigerant mass flow rate at the condenser inlet was 153.6 kg/h, and the refrigerant inlet temperature was 360 K. The air mass flow rate at the inlet was 76 kg/h, and the air inlet temperature was 313 K. The refrigerant inlet pressure was 1428 KPa, the refrigerant side flow resistance was 82.74 Pa, and the air side wind resistance was 252.63 Pa. The measured experimental data and simulation data are shown in Table 3.

Table 3 displays the error analysis between the simulation and experimental data. The results indicate that the simulation closely matches the experimental outcomes. The maximum relative error for the refrigerant outlet temperature difference is under 9.5%, with an average relative error of 7.75%. For the air outlet temperature difference, the maximum relative error is 11.2%, and the average relative error is 8.42%. These minor relative errors validate the feasibility of the condenser simulation method, confirming that the simulation results are suitable for engineering calculations.

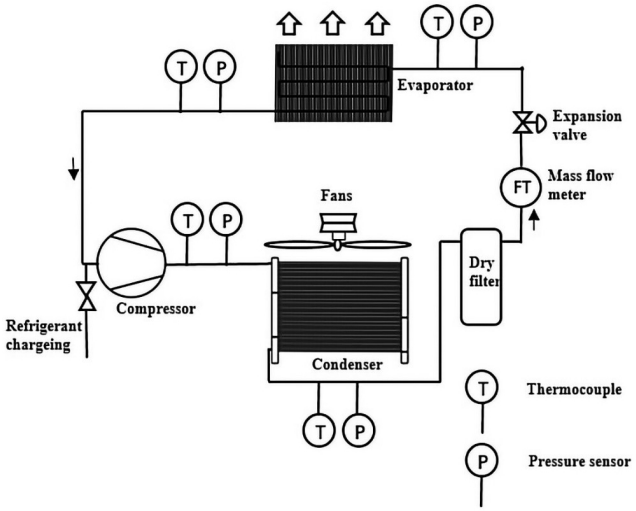

Fig. 4. Experimental test platform for condenser operation system

4.2. Influence of aspect ratio of refrigerant side channel on heat transfer characteristics of the condenser

In this study, five rectangular microchannel refrigerant channels with the same cross-sectional area but varying aspect ratios were selected. The detailed geometric parameters of these channels are listed in Table 4. The condenser refrigerant was introduced

Table 4
Different dimensions of refrigerant channel models at various aspect ratios

Width W (mm)	Height H (mm)	Equivalent diameter D (mm)	Length L (mm)	Aspect ratio H/W
0.45	0.65	0.532	180	1.44
0.55	0.53	0.541	180	0.97
0.65	0.45	0.532	180	0.69
0.75	0.39	0.513	180	0.52
0.80	0.36	0.511	180	0.45

Table 3
Error analysis table of experimental results

Cryogen inlet temperature (K)	Air inlet temperature (K)	Refrigerant outlet temperature (K) (experimental value)	Refrigerant outlet temperature (K) (numerical simulation value)	Temperature difference at refrigerant outlet relative error (%)	Air outlet temperature (K) (experimental value)	Air outlet temperature (K) (numerical simulation value)	Air outlet temperature difference relative error (%)
360.01	307.94	319.37	322.01	6.5	313.26	312.88	7.2
360.49	307.96	319.47	323.38	9.5	313.31	312.71	11.2
360.96	307.96	319.67	322.77	7.6	313.45	313.08	7.5
361.22	307.94	319.89	322.74	6.9	313.48	313.08	7.3
361.99	307.98	319.92	330.02	8.1	313.49	312.97	9.5
362.08	307.96	319.99	323.32	7.9	313.51	313.08	7.8

at an inlet flow rate of 3.2 kg/h and an inlet temperature of 330 K. The airflow rate at the inlet was 9.5 kg/h, with an inlet temperature of 313 K.

Figure 5 illustrates the temperature variation cloud map of the refrigerant for different aspect ratios of the refrigerant channels. As depicted in the figure, across the five different aspect ratios, the distance from the refrigerant to the condensation point is nearly uniform. Additionally, the rate and effectiveness of temperature reduction are relatively consistent among the different aspect ratios.

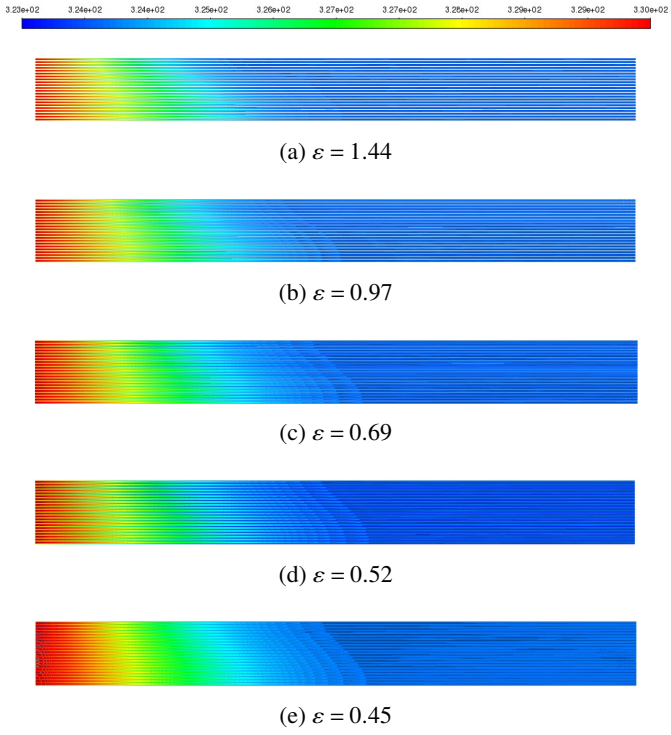

Fig. 5. Contour of refrigerant temperature variation at different aspect ratios of refrigerant channels

Figure 6 displays the cloud maps of the overall and outlet liquid phase volume fractions of the refrigerant under different aspect ratios of the refrigerant channels. As the aspect ratio of the refrigerant channel decreases, both the overall and outlet liquid phase volume fractions first increase and then decrease.

Figure 7 shows the variation curve of the liquid phase volume fraction at the refrigerant outlet with respect to the position within the refrigerant channel. The trend mirrors that observed in Fig. 6, with liquid phase volume fractions initially increasing and then decreasing as the aspect ratio of the refrigerant channel decreases. When the aspect ratio increases from 0.97 to 1.44, condensation capacity decreases by 19.7%. Conversely, when the aspect ratio decreases from 0.97 to 0.45, condensation capacity decreases by 10.0%, 16.2%, and 18.9%, respectively.

Figure 8 illustrates the variation curve of the heat exchange of the condenser with respect to the position within their refrigerant channel. The heat exchange initially increases and then decreases as the aspect ratio of the refrigerant channel decreases. The highest heat exchange is achieved when the aspect ratio is 0.97.

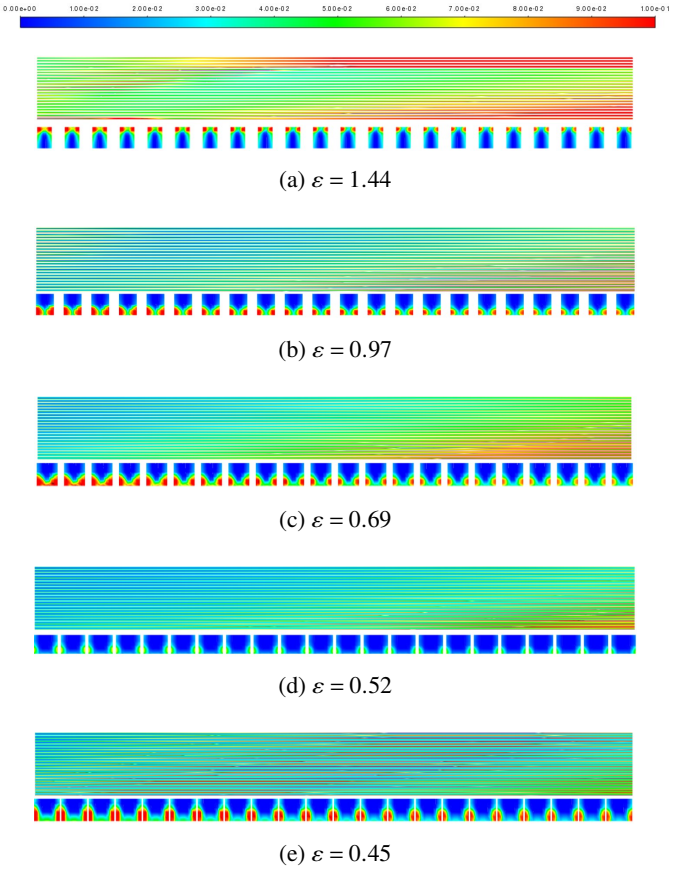

Fig. 6. Distribution of the overall and outlet liquid phase volume fractions of refrigerants with different aspect ratio

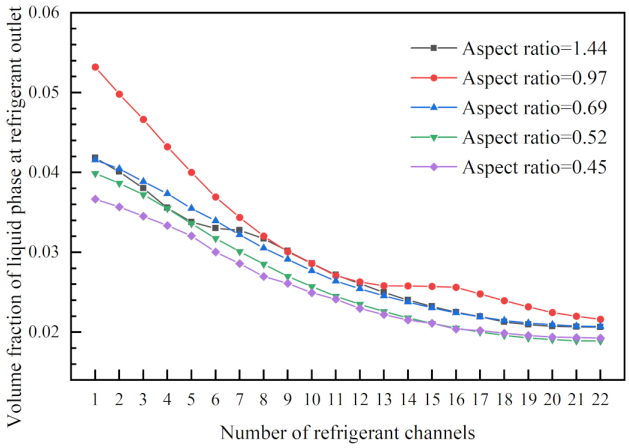

Fig. 7. Liquid phase volume fraction of refrigerant outlet as a function of refrigerant channel position

As the aspect ratio increases from 0.97 to 1.44, the heat transfer rate decreases by 5.6%. When the aspect ratio decreases from 0.97 to 0.45, the heat transfer rate decreases by 5.5%, 6.4%, and 7.3%, respectively.

Figure 9 indicates that the CPE value is maximized, and overall performance is optimized when the refrigerant channel's height-to-width ratio approaches 1. This is because the refriger-

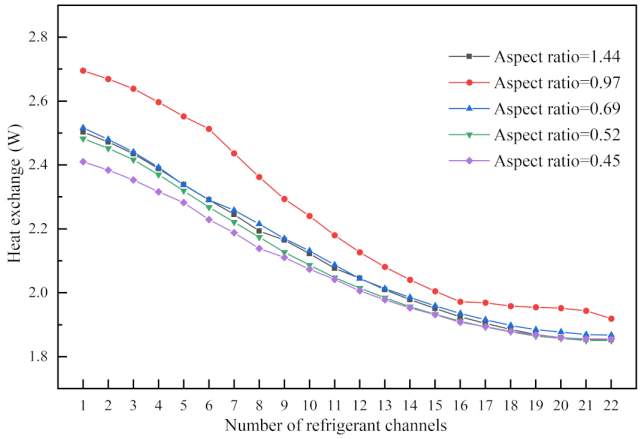

Fig. 8. Heat transfer curve with refrigerant channel position

ant channel shape maximizes the surface area per unit volume, allowing the refrigerant channels to provide more heat transfer area within a given volume. Additionally, when the height-to-width ratio of the refrigerant channel is close to 1, the pressure drop is minimized.

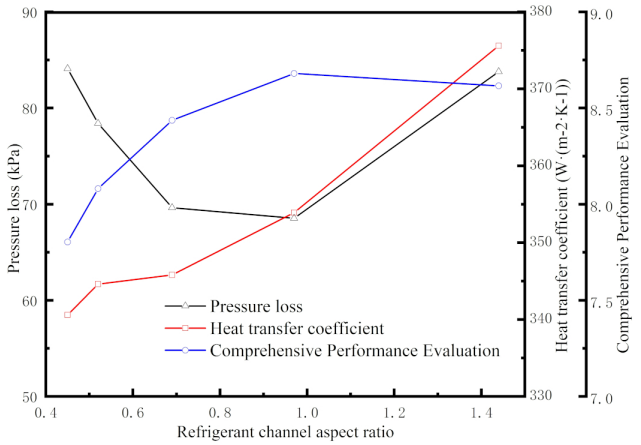

Fig. 9. Comparison of aspect ratio performance of refrigerant side channels

4.3. Influence of the total number of refrigerant channels on the heat transfer characteristics of the condenser

To explore the impact of varying the total number of refrigerant channels on the heat exchange performance of the condenser with a constant refrigerant inlet cross-sectional area, this study uses five rectangular microchannel heat exchangers with identical cross-sectional areas but different numbers of refrigerant channels. Detailed geometric parameters are provided in Table 5. The refrigerant inlet flow rate is 3.2 kg/h at an inlet temperature of 330 K, while the air inlet flow rate is 9.5 kg/h at an inlet temperature of 313 K.

Figure 10 presents the distribution contour of the liquid phase volumetric fraction at the refrigerant outlet for different total numbers of refrigerant channels. Figure 11 shows the variation curve of the liquid phase volumetric fraction at the refrigerant

Table 5
Refrigerant channel models of various sizes for different total quantities

Total amount of refrigerant channels	Width W (mm)	Height H (mm)	Length L (mm)
10	1.43	0.45	180
14	1.02	0.45	180
18	0.79	0.45	180
22	0.65	0.45	180
26	0.55	0.45	180

outlet with respect to the total number of refrigerant channels. As the total number of refrigerant channels increases, the liquid phase volumetric fraction at the refrigerant outlet initially increases and then rapidly decreases. Specifically, when the total number of refrigerant channels increases from 10 to 18, the overall condensation amount of the condenser increases by 0.7% and 10.6%, respectively. However, when the total number of refrigerant channels further increases from 18 to 26, the overall condensation amount decreases by 6.6% and 59.2%, respectively.

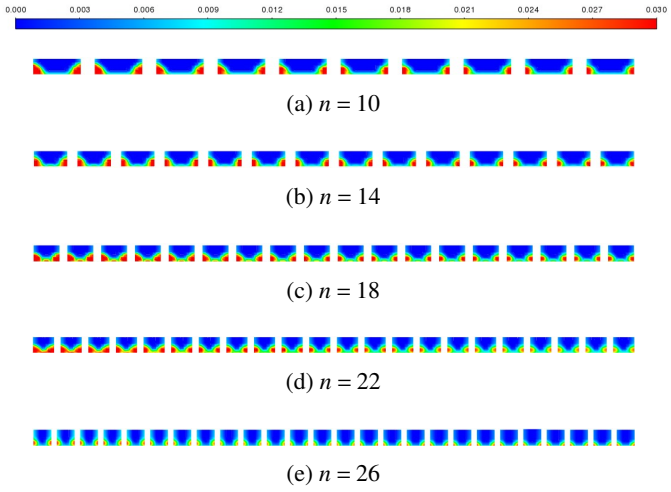

Fig. 10. Distribution of liquid phase volume fraction at the refrigerant outlet under different total quantities of refrigerant channels

Figure 12 illustrates the heat exchange as a function of the total number of refrigerant channels. The heat exchange initially increases slowly and then decreases sharply with the total number of refrigerant channels. When the total number of refrigerant channels increases from 10 to 18, the condenser heat transfer rate rises to 47.4 W, showing an increase of 3.6% and 17.7%, respectively. As the total number of refrigerant channels continues to increase to 26, the heat transfer rate decreases to 31 W, reflecting a decrease of 3.0% and 35.1%, respectively.

With the cross-sectional area of the refrigerant inlet remaining constant, increasing the total number of refrigerant channels results in the fluid flowing across more pipe walls, thereby increasing the heat exchange surface area per unit volume and

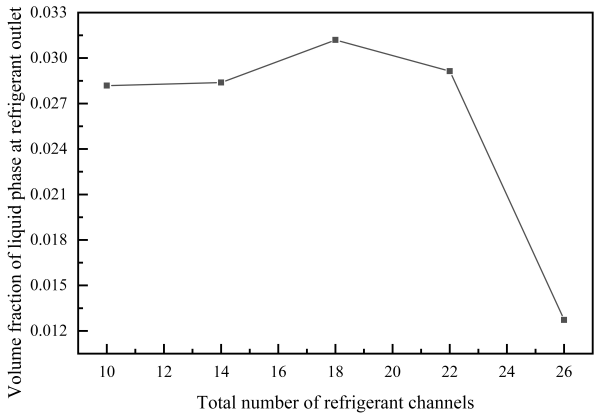

Fig. 11. Curve of variation of liquid phase volume fraction at the refrigerant outlet with the total number of refrigerant channels

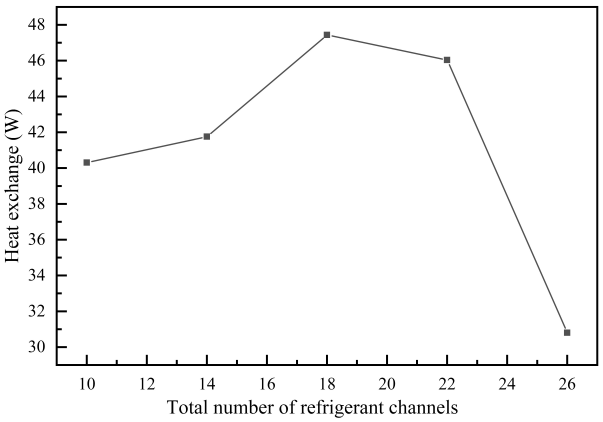

Fig. 12. Curve of heat exchange with the total number of refrigerant channels

enhancing the heat transfer rate. As shown in Fig. 13, when the total number of refrigerant channels increased from 10 to 18, the heat transfer rate improved. The heat transfer coefficient reached its maximum when the total number of refrigerant channels was 22. Further increasing the number of channels leads to a sharp rise in pressure drop within the channels, which deteriorates the heat transfer performance. Figure 13 indicates that

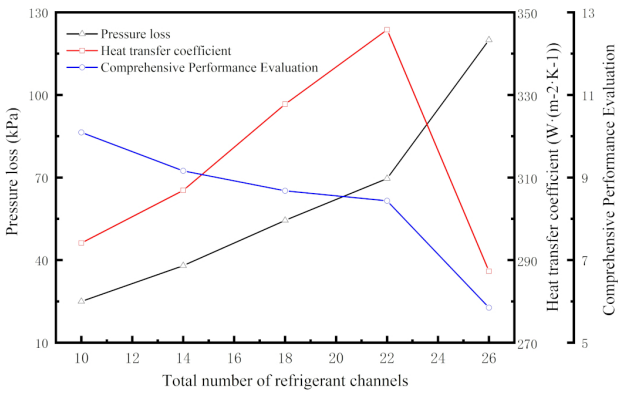

Fig. 13. Comparison of aspect ratio performance of the total number of refrigerant channels

the CPE value decreases with the increase in the total number of refrigerant channels. However, the heat transfer rate and coefficient are optimal when the total number of channels ranges from 18 to 22.

4.4. Influence of the aspect ratio of the wind side on the heat transfer characteristics of the condenser

In a fork-flow condenser, the fin is a key component whose structural parameters significantly impact the heat transfer and mass transfer performance of the condenser. After simulating the effects of the aspect ratio of the R134a refrigerant channels on the heat transfer characteristics of the condenser, it is essential to investigate further how different fin configurations affect the condenser's heat exchange performance. To compare the heat transfer performance of condensers with varying ratios of aspect, this simulation examines five fin aspect ratios: 2.36, 2.87, 3.56, 4.53 and 5.96. The detailed geometric parameters of these configurations are listed in Table 6. The condenser operates with a refrigerant inlet flow rate of 3.2 kg/h and an inlet temperature of 330 K. The air inlet flow rate is 9.5 kg/h with an inlet temperature of 313 K.

Table 6
Refrigerant channel models of different sizes for various quantities

Air duct width W_1 (mm)	Fin height H (mm)	Fin width W_2 (mm)	Number of air ducts	Aspect ratio H/W
1.08	2.55	0.07	155	2.36
0.98	2.81	0.17	155	2.87
0.88	3.13	0.27	155	3.56
0.78	3.53	0.37	155	4.53
0.68	4.05	0.47	155	5.96

This approach will help in understanding how varying fin aspect ratios impact the overall heat exchange efficiency of the condenser. As the fin aspect ratio increases, the superheated region of the refrigerant also gradually expands while the phase-change heat transfer region shortens. For larger aspect ratios, the refrigerant in the channels requires a longer distance and time to reach the phase-change temperature. When the aspect ratios are 2.87, 3.56, and 4.53, the superheated regions are relatively similar when the refrigerant reaches the phase-change temperature. However, further increasing the aspect ratio results in a noticeable extension of the superheated region.

Figure 14 illustrates the variation in the heat exchange of the condenser as a function of the number of the refrigerant channels. The heat exchange increases continuously with the rising fin aspect ratio. Specifically, as the fin aspect ratio increases from 2.36 to 5.96, the heat transfer rate rises by 6.62%, 11.3%, 17.8%, and 20.6%, respectively. An increase in the fin aspect ratio implies a larger space for airflow, allowing more air to pass through the fins. This enhanced airflow capacity contributes to improved heat transfer performance, as more air can interact

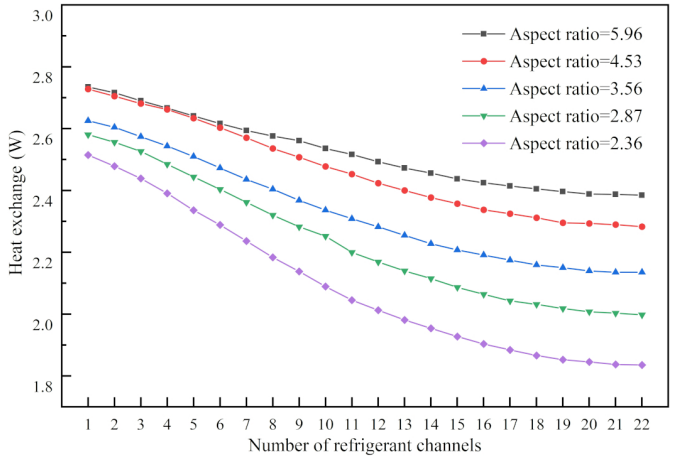

Fig. 14. Heat exchange curve with the number of the refrigerant channels

with the fin surfaces, enhancing the overall heat exchange process.

Figure 15 shows the variation in the liquid phase volume fraction of the refrigerant at the outlet as a function of the number of the refrigerant channels. As the fin aspect ratio increases, the liquid phase volume fraction at the refrigerant outlet rises steadily. Specifically, with an increase in the fin aspect ratio from 2.36 to 5.96, the liquid phase volume fraction increases by 14.2%, 27.1%, 43.4%, and 57.8%, respectively. This trend indicates that a higher fin aspect ratio leads to a more significant proportion of liquid refrigerant exiting the condenser, likely due to improved heat exchange and extended condensation processes.

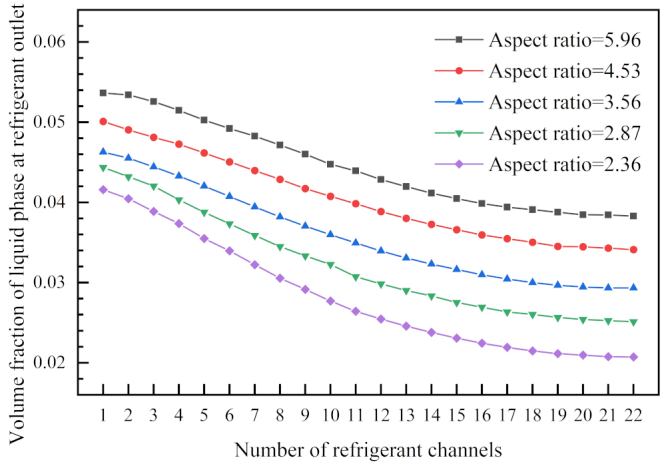

Fig. 15. Volume fraction of the liquid phase at the refrigerant outlet as a function of the position of the refrigerant channel

Figure 16 depicts the heat transfer coefficient curve, which aligns with the CPE curve, showing that CPE is maximized when the fin aspect ratio is 4.53. At this aspect ratio, the pressure drop is relatively low, leading to the most effective heat transfer performance. This indicates that the optimal fin aspect ratio balances efficient heat transfer with minimal pressure loss, achieving the best overall performance for the condenser.

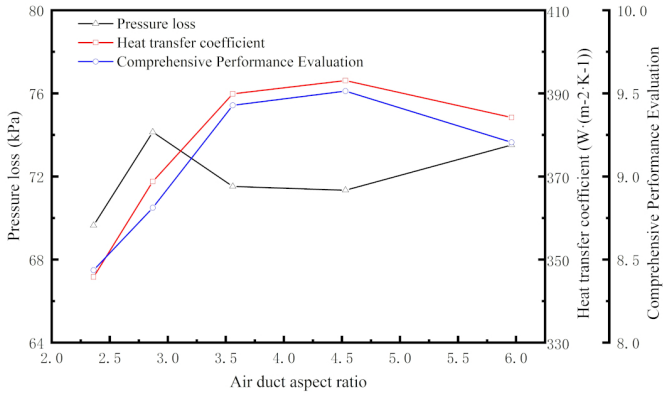

Fig. 16. Comparison of air duct aspect ratio performance

5. CONCLUSIONS

This article presents a periodic iteration method for simulating the single-process heat transfer characteristics of a fork-flow condenser in a two-phase region, enabling the numerical simulation of extensive models. The main findings are:

1. When the number of periodic iterations for the condenser in the two-phase region does not exceed three, the relative error in the refrigerant outlet temperature difference remains within 0.19%, the heat exchange error within 0.76%, and the condensation rate relative error within 1.02%. This high level of accuracy indicates that the cyclic iteration method is feasible and effective.
2. The study found that when using R134a as the refrigerant, both the condensation and heat transfer rates initially increase and then decrease as the refrigerant channel aspect ratio increases. Maximum heat transfer and condensation rates, along with the highest CPE factor, occur when the aspect ratio is close to 1, ensuring the best condenser performance with the lowest pressure drop. On the airside, heat transfer characteristics improve initially and then weaken with increasing fin aspect ratio. Optimal performance is achieved at an aspect ratio of 4.53, where the pressure loss is minimized, and the CPE value is maximized.
3. Regarding changes in the total number of refrigerant-side channels, the heat transfer characteristics initially strengthen and then weaken as the total number of channels increases. The study results indicate that optimal performance of the model occurs when the total number of channels is between 18 and 22. Increasing the total number of channels beyond this range leads to increased pressure drop and worsened heat transfer performance.

REFERENCES

[1] R. Wang, T. Sun, A.-E. Polzin, and S. Kabelac, "Experimental investigation of the two-phase local heat transfer coefficients for condensation of R134a in a micro-structured plate heat exchanger," *Heat Mass Transf.*, vol. 58, no. 1, pp. 1–18, Jan. 2022, doi: 10.1007/s00231-021-03091-0.

[2] P. Behnam, A. Shafieian, M. Zargar, and M. Khiadani, "Performance enhancement of a solar-driven DCMD system using an

air-cooled condenser and oil: Experimental and machine learning investigations," *Desalination*, vol. 574, p. 117255, Apr. 2024, doi: 10.1016/j.desal.2023.117255.

[3] G. Peker and D. Burcu Özkan, "Performance evaluation of hot-wall condenser in a domestic refrigerator," *Appl. Therm. Eng.*, vol. 233, p. 121137, Oct. 2023, doi: 10.1016/j.applthermaleng.2023.121137.

[4] F. Erdem Şahnali, Ş.Ö. Atayılmaz, and Z. Gemici, "Numerical analysis of the heat transfer and pressure drop of a wavy fin and Kammtail tube condenser: An investigative study," *Case Stud. Therm. Eng.*, vol. 55, p. 104191, Mar. 2024, doi: 10.1016/j.csite.2024.104191.

[5] R.S. Espíndola, J. Boeng, F.T. Knabben, and C.J.L. Hermes, "A new heat transfer correlation for natural draft wire-on-tube condensers for a broad geometry span," *Int. J. Refrig.*, vol. 114, pp. 10–18, Jun. 2020, doi: 10.1016/j.ijrefrig.2020.02.025.

[6] S. M. Ammar, Z. Ramadan, and C.W. Park, "Performance evaluation of novel plate-type condenser for an absorption/adsorption refrigeration syem: Experimental and CFD study," *Case Stud. Therm. Eng.*, vol. 56, p. 104260, Apr. 2024, doi: 10.1016/j.csite.2024.104260.

[7] Y.-Y. Yan and T.-F. Lin, "Condensation heat transfer and pressure drop of refrigerant R-134a in a small pipe," *Int. J. Heat Mass Transf.*, vol. 42, no. 4, pp. 697–708, Feb. 1999, doi: 10.1016/S0017-9310(98)00195-1.

[8] L. Chamra and R. Webb, "A Review on Condensation and Evaporation in Micro-fin Tubes at Equal Saturation Temperatures," *J. Enhanc. Heat Transf.*, vol. 24, no. 1–6, pp. 399–409, 2017, doi: 10.1615/JEnhHeatTransf.v24.i1-6.290.

[9] K. Chung, K.-S. Lee, and W.-S. Kim, "Optimization of the design factors for thermal performance of a parallel-flow heat exchanger," *Int. J. Heat Mass Transf.*, vol. 45, no. 24, pp. 4773–4780, Nov. 2002, doi: 10.1016/S0017-9310(02)00195-3.

[10] C.W. Bullard, J. Proctor, J. Brezner, K.B. Mercer, and R.A. Davis, "Modeling and testing of a utility peak reducing residential hot/dry air conditioner (HDAC) using microchannel heat exchangers," *ASHRAE Trans.*, vol. 112, p. 162, 2006.

[11] A. Cavallini, D. Del Col, L. Doretti, M. Matkovic, L. Rossetto, and C. Zilio, "Two-phase frictional pressure gradient of R236ea, R134a and R410A inside multi-port mini-channels," *Exp. Therm. Fluid Sci.*, vol. 29, no. 7, pp. 861–870, Aug. 2005, doi: 10.1016/j.expthermflusci.2005.03.012.

[12] M. Zhang and R.L. Webb, "Correlation of two-phase friction for refrigerants in small-diameter tubes," *Exp. Therm. Fluid Sci.*, vol. 25, no. 3–4, pp. 131–139, Oct. 2001, doi: 10.1016/S0894-1777(01)00066-8.

[13] R. Webb and K. Ermis, "Effect of hydraulic diameter on condensation of R-134A in flat, extruded aluminum tubes," *J. Enhanc. Heat Transf.*, vol. 8, no. 2, pp. 77–90, 2001, doi: 10.1615/JEnhHeatTransf.v8.i2.20.

[14] C.-C. Wang, W.-H. Tao, and C.-J. Chang, "An investigation of the airside performance of the slit fin-and-tube heat exchangers," *Int. J. Refrig.*, vol. 22, no. 8, pp. 595–603, Dec. 1999, doi: 10.1016/S0140-7007(99)00031-6.

[15] X. Du, M. Zeng, Q. Wang, and Z. Dong, "Experimental Investigation of Heat Transfer and Resistance Characteristics of a Finned Oval-Tube Heat Exchanger With Different Air Inlet Angles," *Heat Transf. Eng.*, vol. 35, no. 6–8, pp. 703–710, May 2014, doi: 10.1080/01457632.2013.837780.

[16] N.-H. Kim, "Effects of fin corrugation and tube geometry on the airside performance of fin-and-tube heat exchangers – Part I: dry surface," *J. Therm. Sci. Technol.*, vol. 16, no. 2, p. JTST0031, 2021, doi: 10.1299/jtst.2021jtst0031.

[17] J.M. Saiz Jabardo, J.R. Bastos Zoghbi Filho, and A. Salamanca, "Experimental study of the air side performance of louver and wave fin-and-tube coils," *Exp. Therm. Fluid Sci.*, vol. 30, no. 7, pp. 621–631, Jul. 2006, doi: 10.1016/j.expthermflusci.2006.01.001.

[18] K. Ryu and K.-S. Lee, "Generalized heat-transfer and fluid-flow correlations for corrugated louvered fins," *Int. J. Heat Mass Transf.*, vol. 83, pp. 604–612, Apr. 2015, doi: 10.1016/j.ijheatmasstransfer.2014.12.044.

[19] Z. Liu, J. Zhao, C. Wang, Y. Qin, Y. Wang, and C. Liu, "Numerical investigations on the thermal performance of two-phase closed thermosyphon with extended condenser surface," *Heat Mass Transf.*, Jul. 2022, doi: 10.1007/s00231-022-03264-5.

[20] J.U. Brackbill, D.B. Kothe, and C. Zemach, "A continuum method for modeling surface tension," *J. Comput. Phys.*, vol. 100, no. 2, pp. 335–354, Jun. 1992, doi: 10.1016/0021-9991(92)90240-Y.